Supporting Information

Tunable Near-infrared Emission and Three-Photon Absorption in Lanthanide-doped Double Perovskite Nanocrystals

Md Soif Ahmed,[a] Lavadiya Sireesha,[a] Sudhanshu Kumar Nayak,[a] Rangarajan Bakthavatsalam,[b] Dipanjan Banerjee,[c] Venugopal Rao Soma,[c] Janardan Kundu,[b] Sai Santosh Kumar Raavi[a,d]*

[a] *Ultrafast Photo-physics and Photonics Laboratory, Department of Physics, Indian Institute of Technology Hyderabad, Kandi 502285, Telangana, India*

[b] *Indian Institute of Science Education and Research (IISER) Tirupati, Tirupati, Andhra Pradesh 517507, India*

[c] *Advanced Centre of Research in High Energy Materials (ACRHEM), DRDO Industry Academia – Centre of Excellence (DIA-COE), University of Hyderabad, Hyderabad 500046, Telangana, India*

[d] *Department of Climate Change, Indian Institute of Technology Hyderabad, Kandi 502285, Telangana, India*

Corresponding author e-mail address: **sskraavi@phy.iith.ac.in**

Synthesis of double perovskite nanocrystals (DPNCs)

The undoped and rare-earth doped $Cs_2AgInCl_6$ double perovskite nanocrystals were synthesized following the same method as reported previously in literatures[1-3].

Chemicals: Cesium carbonate (Cs_2CO_3, 99.9%), Oleic acid (OA >85%), Oleyl amine (OLA, 70%), Silver acetate (Ag(ac), 99.0%), Indium acetate ($In(ac)_3$, 99.99%), Erbium acetate ($Er(ac)_3$, 99.9%), Ytterbium acetate ($Yb(ac)_3$, 99.95%), Diphenyl ether (DPE, 99%), Benzoyl chloride (Bz-Cl, 99%), n-Hexane (99%). All chemicals were purchased from Sigma-Aldrich and used without any further purification.

Preparation of Cesium oleate: The precursor of Cs-oleate was prepared by adding 1630 mg of cesium carbonate with 20 ml of oleic acid into a three neck flask RB and this mixer was first degassed by using the vacuum pump at 100^o C for 2 hours and the temperature is subsequently increased to 150^o C under the nitrogen flux for 3 hours to get the clear solution. The obtained precursor is cooled down to room temperature and stored in an inert atmosphere.

Synthesis of DPNCs: The lead-free undoped and doped $Cs_2AgInCl_6$ double perovskite nanocrystals were prepared by using the hot-injection method. The reaction was prepared by mixing 0.24 mmol of silver acetate, 0.25 mmol of indium acetate, 1mL of Cs-oleate, 0.5 mL of oleylamine and 4 mL of diphenyl ether into a three-neck RB flask and this reaction was degassed under vacuum for 30 min at 40^o C. After degassing the reaction was kept under nitrogen flux and the temperature was increased to 105^o C at the rate of 10^o C/min. 0.5 mL of degassed DPE was mixed with 200 µL of Benzoyl chloride and the mixture was swiftly injected into the RB flask; after 5 seconds, the reaction was quenched and kept under ice-water bath. The obtained crude solution was transferred into centrifuge tubes and centrifuged at 4500 rpm for 10 mins, the supernatant was discarded, and the precipitated nanocrystals were collected and dispersed into the 3 mL hexane to get the colloidal solution.

The Erbium (Er) and Ytterbium(Yb) doped $Cs_2AgInCl_6$ NCs were synthesized by following the same protocol as undoped NCs preparation, but adding the proper amount of ytterbium acetate or erbium acetate to the reaction mixture. We took the feed ratios Yb/In = 20% for Yb-doped NC (Yb-DP) and Er/In = 20% for Er-doped NC (Er-DP).

Photophysical characterizations

UV-vis absorption:

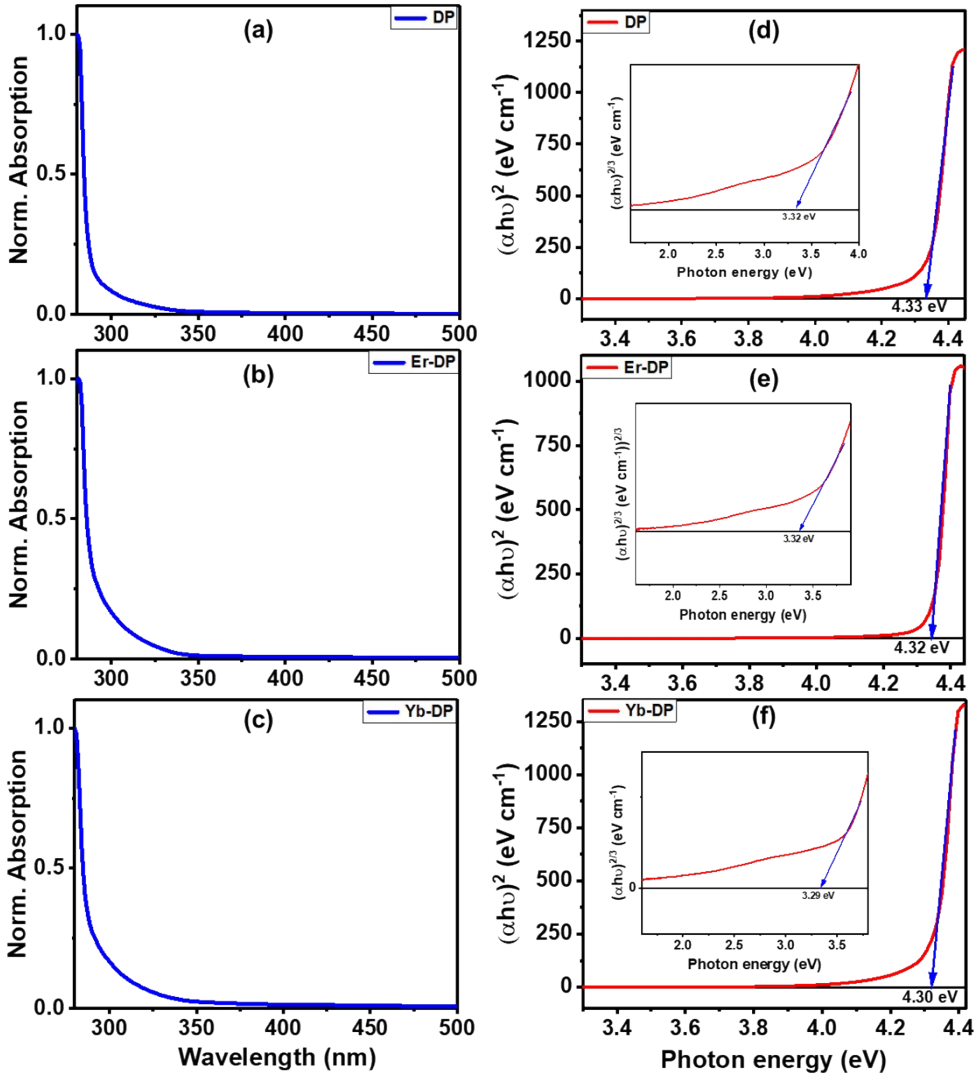

Fig. S1 UV-visible absorption spectra of (a) DP, (b) Er-DP and (c) Yb-DP. Tauc plots for the strong transition in the NC absorption of (d) DP, (e) Er-DP and (f) Yb-DP. The insets show the Tauc plots for the weak band edge transition.

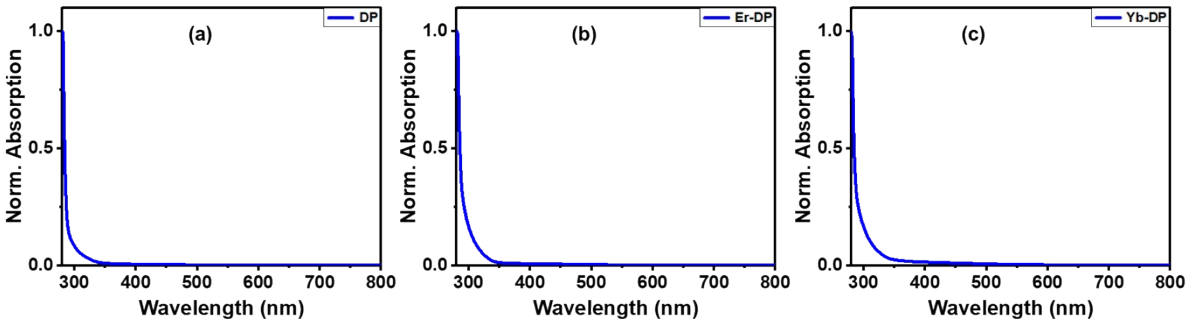

Fig. S2 UV-visible absorption spectra of (a) DP, (b) Er-DP and (c) Yb-DP, shows upto 800 nm.

Photoluminescence (PL):

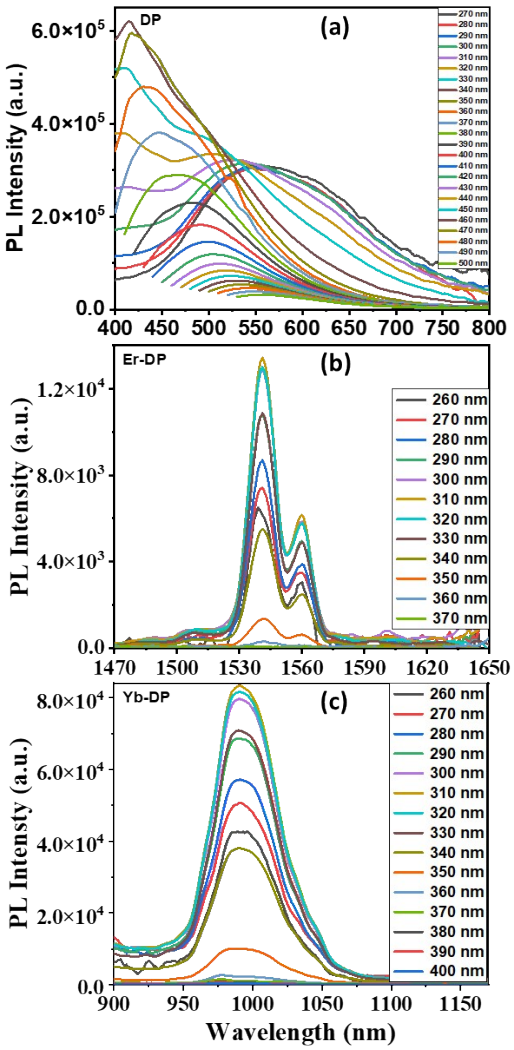

Fig. S3 Excitation wavelength dependent PL spectra at room temperature for (d) DP, (e) Er-DP and (f) Yb-DP.

Photoluminescence Excitation (PLE):

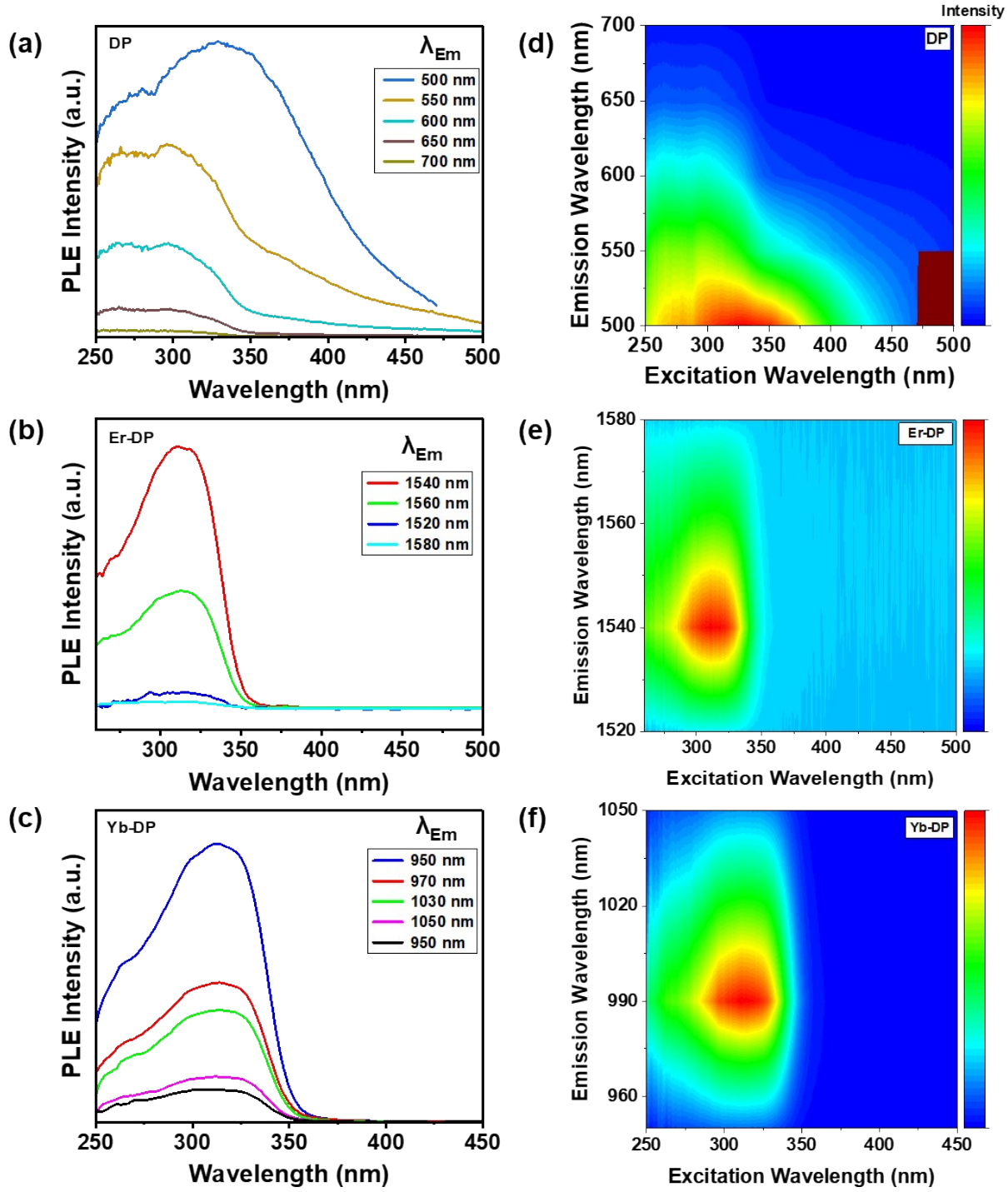

Fig. S4 PLE spectra of (a) DP, (b) Er-DP and (c) Yb-DP at different emission wavelengths (λ_{Em}). (c), (e) and (f)- corresponding pseudocolor plot of the PLE maps.

Photoluminescence (PL) of Er-DP and Yb-DP in visible region:

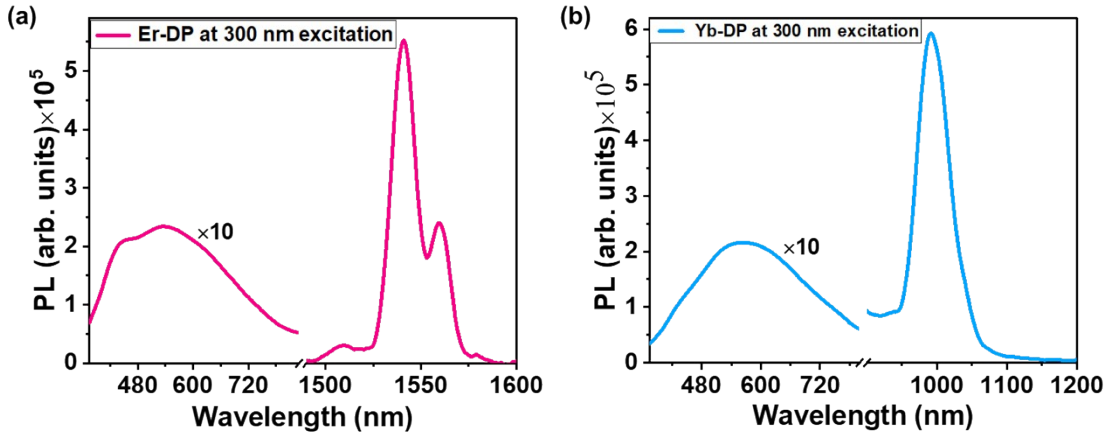

Fig. S5 Visible and near infrared regions PL curves of (a) Er-DP and (b) Yb-DP at the excitation wavelength of 300 nm.

Temperature-dependent photoluminescence of DP:

The full width half maxima (FWHM) increased abruptly at higher temperatures. Therefore, to get a good fitting of FWHM vs temperature (T) data, we took the data point upto 160 K to obtain the Huang–Rhys factor (S).

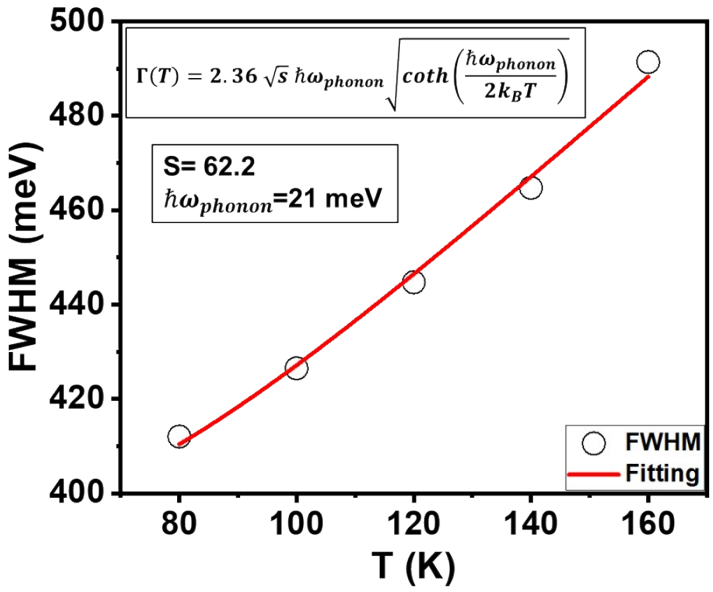

Fig. S6 FWHM vs temperature data of DP. Scattered symbols represent experimental data, and solid red line is the theoretical fitting.

Time-resolved photoluminescence (TRPL):

We implemented the time-correlated single photon counting (TCSPC) experiment to obtain the TRPL of DP.

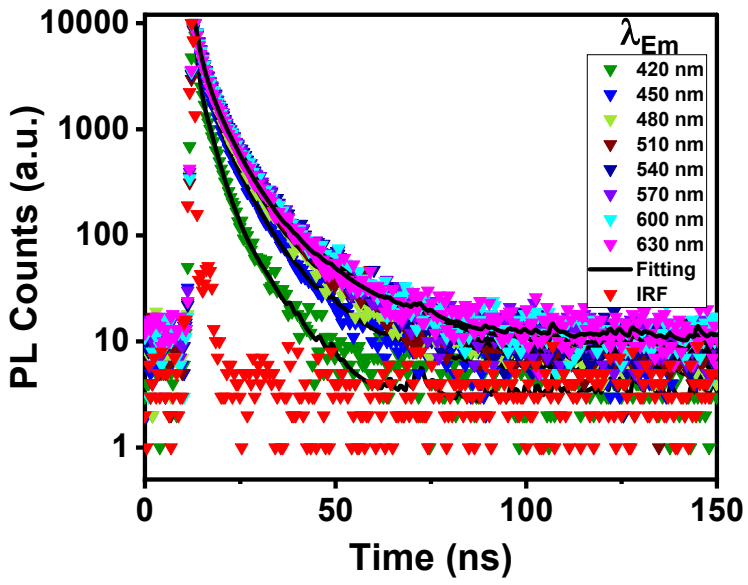

Fig. S7 TRPL of DP at the different emission wavelengths at room temperature.

Table S1 PL decay components and average lifetimes at various emission wavelengths of DP at room temperature.

λ_{Em} (nm)	τ_1 (ns)	Rel. %	τ_2 (ns)	Rel. %	τ_3 (ns)	Rel.%	$\chi 2$	τ_{avg} (ns)
420	0.6772	38.24	2.792	48.38	8.160	13.38	1.3772	2.65
450	1.446	46.11	5.086	47.24	16.01	6.65	1.2910	4.13
480	1.436	37.40	5.191	53.55	17.57	9.05	1.2696	4.90
510	1.564	37.60	5.606	52.18	16.64	10.22	1.2496	5.22
540	1.554	34.88	5.476	51.84	16.19	13.28	1.4893	5.53
570	1.309	28.55	4.940	55.40	14.80	16.06	1.2598	5.48
600	1.372	33.21	5.065	52.97	15.90	13.82	1.2784	5.34
630	1.345	39.39	5.207	49.88	16.45	10.72	1.1838	4.89

Table S2 PL decay components and average lifetimes at various emission wavelengths of DP at 77 K.

λ_{Em} (nm)	τ_1 (ns)	Rel. %	τ_2 (ns)	Rel. %	τ_3 (ns)	Rel.%	$\chi 2$	τ_{avg} (ns)
420	1.273	51.01	3.845	45.12	16.86	3.87	1.2533	3.04
450	1.678	42.66	4.878	48.49	15.54	8.84	1.2152	4.46
480	1.713	30.52	5.108	54.91	15.31	14.57	1.1871	5.56
510	2.299	50.64	6.571	41.43	19.91	7.93	1.3406	5.62
540	2.293	38.92	6.795	51.77	21.41	9.31	1.1111	6.41
570	1.999	47.12	6.273	44.38	18.15	8.50	1.2578	5.27
600	2.331	60.12	6.737	34.42	19.91	5.47	1.3278	4.81

Temperature-dependent photoluminescence of Er-DP:

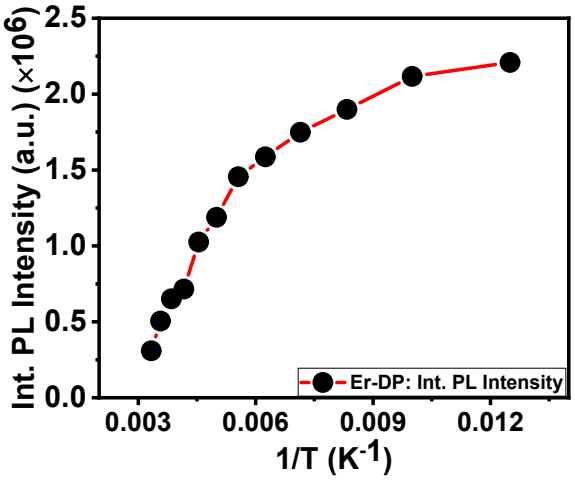

Fig. S8 Integrated PL intensity vs temperature curve of Er-DP. Scattered symbols are experimental data and solid red line is the theoretical fitting.

Nonlinear optical properties

Assuming Gaussian beam profile, the general equation for normalized energy transmittance given by Sutherland et al. [4-6] using the open aperture Z-scan theory for multiphoton absorption is described as

$$T_{OA(nPA)} = \frac{1}{\left[1 + (n-1)\alpha_n L_{eff}\left(\frac{I_0}{1+\left(\frac{z}{z_0}\right)^2}\right)^{n-1}\right]^{\frac{1}{n-1}}} \quad \text{(S1)}$$

where α_n is the nonlinear MPA coefficient of the sample like how n = 2 for two-photon absorption (2PA), $n = 3$ for 3PA, and so on. L_{eff} is the effective path length of the sample, $z_0 = \frac{\pi\omega_0^2}{\lambda}$ is the Rayleigh range, z is sample position with respect to the focusing lens, ω_0 is the beam width at the focal point, and I_0 is the input peak irradiance at the focus.

We employed the following analytical equations for fitting the 2PA and 3PA to OA Z-scan data by choosing n = 2 and n = 3,

$$T_{OA(2PA)} = \frac{1}{1 + \alpha_2 L_{eff}\left(\frac{I_0}{1+(z/z_0)^2}\right)}. \quad \text{(S2)}$$

$$T_{OA(3PA)} = \frac{1}{\left[1 + 2\alpha_3 L_{eff}^{'}\left(\frac{I_0}{1+\left(\frac{z}{z_0}\right)^2}\right)^2\right]^{\frac{1}{2}}} \quad \text{(S3)}$$

In the above equations α_2 is 2PA coefficient and α_3 is 3PA coefficient. $L_{eff} = \frac{1 - e^{-\alpha_0 L}}{\alpha_0}$ and $L_{eff}^{'} = \frac{1 - e^{-2\alpha_0 L}}{2\alpha_0}$ are the effective path length of the sample for 2PA, and 3PA, respectively where α_0 is the linear absorption coefficient.

Equation for theoretical fit of close aperture Z-scan data [7]:

$$T_{CA}(x) = 1 + \frac{4x\Delta\Phi}{(1+x^2)(9+x^2)} + \frac{4(3x^2-5)\Delta\Phi^2}{(1+x^2)(9+x^2)(25+x^2)} + \frac{}{(1} \quad \text{(S4)}$$

.

Here, $T_{CA}(x)$ is the normalised transmittance, $x = -z/z_0$, z is the sample's longitudinal distance from the focus point (z=0), z_0 is the Raleigh range and $\Delta\Phi$ is the on-axis nonlinear phase shift.

The relationship [8, 9] that was utilised to determine $\langle\gamma\rangle$:

$$\langle\gamma\rangle = \frac{\chi^{(3)}}{NL^4}, \quad \text{(S5)}$$

where $\chi^{(3)}$ is the third-order nonlinear susceptibility, N is the number density of molecule in solution samples, and the local field factor is $L = \frac{n_0^2 + 2}{3}$.

In the two-band model, the band edge effective masses for the conduction m_c and valence bands m_v are given by[10]

$$\frac{m_0}{m_c} = 1 + \frac{E_p}{3E_g}, \tag{S6}$$

$$\frac{m_0}{m_v} = -1 + \frac{E_p}{3E_g}. \tag{S7}$$

In the above equations, m_0 is the free-electron mass and E_g is the band-gap energy. The Kane energy is given by[11]

$$E_p = \frac{2\,|P|^2}{m_0}, \tag{S8}$$

where P is called Kane parameter, is a physical parameter and is a pure real number. If we consider $|c\rangle$ and $|v\rangle$ as the states of the conduction and valence bands, respectively, the eigenstates of the valence band and the conduction band can be expressed as follows[10]

$$|v+,k\rangle = cos\frac{\theta}{2}|v+\rangle + sin\frac{\theta}{2}e^{i\phi}|v-\rangle, \tag{S9}$$

$$|v-,k\rangle = sin\frac{\theta}{2}|v+\rangle - cos\frac{\theta}{2}e^{i\phi}|v-\rangle, \tag{S10}$$

$$|c+,k\rangle = cos\frac{\theta}{2}|c+\rangle + sin\frac{\theta}{2}e^{i\phi}|c-\rangle, \tag{S11}$$

$$|c-,k\rangle = sin\frac{\theta}{2}|c+\rangle - cos\frac{\theta}{2}e^{i\phi}|c-\rangle, \tag{S12}$$

Here, $k = k(cos\phi\ sin\theta, sin\phi\ sin\theta,\ cos\theta)$ with ϕ and θ being the azimuthal and polar angles, respectively.

The relation between the Kane energy E_p and the exciton reduced mass μ and can be obtained from eqn. (S1) and (S2),

$$\frac{m_0}{\mu} = \frac{m_0}{m_c} + \frac{m_0}{m_v} = \frac{2E_p}{3E_g}. \quad \text{(S13)}$$

Therefore, $\mu = m_0 \frac{2E_p}{3E_g}$.

References

1. F. Locardi, M. Cirignano, D. Baranov, Z. Dang, M. Prato, F. Drago, M. Ferretti, V. Pinchetti, M. Fanciulli and S. Brovelli, *Journal of the American Chemical Society*, 2018, 140, 12989-12995.
2. Y. Mahor, W. J. Mir and A. Nag, *The Journal of Physical Chemistry C*, 2019, 123, 15787-15793.
3. W. Lee, S. Hong and S. Kim, *The Journal of Physical Chemistry C*, 2019, 123, 2665-2672.
4. M. Sheik-Bahae, A. A. Said, T.-H. Wei, D. J. Hagan and E. W. Van Stryland, *IEEE journal of quantum electronics*, 1990, 26, 760-769.
5. R. S. S. Kumar, S. V. Rao, L. Giribabu and D. N. Rao, *Chemical Physics Letters*, 2007, 447, 274-278.
6. R. L. Sutherland, *Handbook of nonlinear optics*, CRC press, 2003.
7. M. S. Ahmed, C. Biswas, D. Banerjee, P. Chetti, J.-S. Yang, V. R. Soma and S. S. K. Raavi, *Frontiers in Physics*, 2022, 549.
8. S. V. Rao, N. N. Srinivas, D. N. Rao, L. Giribabu, B. G. Maiya, R. Philip and G. R. Kumar, *Optics Communications*, 2000, 182, 255-264.
9. C. Biswas, N. K. Katturi, N. Duvva, L. Giribabu, V. R. Soma and S. S. K. Raavi, *The Journal of Physical Chemistry C*, 2020, 124, 24039-24051.

10. K. Ohara, T. Yamada, H. Tahara, T. Aharen, H. Hirori, H. Suzuura and Y. Kanemitsu, *Physical Review Materials*, 2019, 3, 111601.

11. P. C. Sercel, J. L. Lyons, N. Bernstein and A. L. Efros, *The Journal of Chemical Physics*, 2019, 151, 234106.